Electrospinning of Liquefied Banana Stem Residue in Conjugation with Hydroxyapatite Nanocrystals: Towards New Scaffolds for Bone Tissue Engineering

Mehdi Sadat-Shojai (msadatshojai@gmail.com)
Shiraz University https://orcid.org/0000-0002-9433-4508
Milad Asadnia
Shiraz University

Research Article

Keywords: Nanofibers, Banana pseudo-stem, DOE, Cellulose, Hydroxyapatite

Posted Date: November 16th, 2021

DOI: https://doi.org/10.21203/rs.3.rs-969607/v1

Version of Record: A version of this preprint was published at Cellulose on March 22nd, 2022. See the published version at https://doi.org/10.1007/s10570-022-04542-5.

Abstract

Electrospun fibers have high structural similarity to the extracellular matrix (ECM) of natural bone. Some researchers have tried to fabricate cellulose nanofibers using electrospinning method, although the fabricated fibers usually exhibited a non-uniform texture. Moreover, the fabricated mats always suffer from low biological, mechanical and structural properties. Thus, the objective of this study was first to produce a naturally occurring cellulose from banana pseudo-stem through the combination of liquefaction and bleaching processes. The native cellulose was then tried to electrospun in order to determine how a systematic approach based on a Taguchi L_9 orthogonal array can be used to fabricate a defect-free fibrous mat. Finally, the electrospun cellulose mats incorporated with hydroxyapatite (HA) nanoparticles were fabricated to generate a new fibrous nanocomposite with enhanced biological and mechanical characteristics. The results revealed that among the electrospinning parameters, cellulose concentration of solution and applied voltage had the greatest effect on the morphology of the fibers. The morphological characterization of the fibrous nanocomposites showed that fibrous cellulose/HA mats had a uniform fiber texture without any significant bead, splashing or particle agglomeration. According to the mechanical tests, the samples containing the higher concentration of HA had a significantly higher elastic modulus and tensile strength. The results obtained from bioactivity analysis indicated an interesting morphological transformation into a flake-like structure which confirmed the high bioactivity of the scaffolds. Accordingly, encapsulation of HA nanoparticles inside the cellulose in the fibrous form can be promising for bone regeneration applications.

Introduction

Bone is reported to be the second most transplanted tissue only behind blood, with over four million operations annually using bone grafts and substitutes to treat complex bone defects (Turnbull et al. 2018). However, several limitations affect current treatment options and hence significant researches in the field of bone tissue engineering have been directed towards developing novel functional alternatives to traditional bone substitutes. This can be achieved by creating porous and bioactive three-dimensional (3D) scaffolds that can induce osteoconduction and integration to support bone regeneration (Perić Kačarević et al. 2020; Turnbull et al. 2018). A variety of biomaterials have been used to this end, each with their own advantages and disadvantages. However, the “perfect” scaffold has not yet been created and clinical translation of bioative scaffolds has been limited as a result.

Bone is a heterogeneous composite material comprising hydroxyapatite (HA) phase, a mixed polymer-based organic phase and water (Sato 2007). During bone scaffold manufacture it would therefore seem promising to include a combination of natural polymers with bioceramics, especially HA minerals, to create a composite scaffold, potentially allowing favorable scaffold bioactivity and strength as well as structural biomimicry to be achieved. Indeed, natural polymers often contain biofunctionality on their surface that can positively support cell adhesion and function on the scaffold (Sadat-Shojai 2018; Turnbull et al. 2018). Polymers with biological origin are also inexpensive and eco-friendly to the environment and their combination with HA can provide further benefits including increased bioactivity

with a more tunable biodegradation rate (Perić Kačarević et al. 2020; Sadat-Shojai 2018; Sayed et al. 2018). Although naturally occurring polymers have been attracted interest of scientists, however, biopolymers based on synthetic materials have usually been incorporated with HA in recent years, and only a few reports are currently available on the bioactive HA nanoparticles in combination with naturally occurring polymers for application in bone reconstruction.

Of a diverse natural polymers, cellulose, produced from plants, animals or bacteria, is considered as one of the world's most popular natural and renewable resource of raw material for environmentally friendly and biocompatible products (Kalia et al. 2011; Meng et al. 2019). Cellulose is constructed from repeating 1,4-β-hydroglucose units connected to each other by β-ether linkages (Kalia et al. 2011). However, despite the enormous potential of cellulose in biomedicine, there are several important issues that remain to be addressed, such as their suboptimal mechanical properties, lack of tuneability of degradation rates and poor processability. On the other hand, most of the studies on cellulose were conducted on various derivatives of cellulose which are poor in strength and susceptible to rapid degradation and usually require some post-modification processes for tissue engineering applications.

From structural point of view, polymeric nanofibers have received extensive interests in recent years due to their similarity with nanoscaled fibrils found in natural extracellular matrix (ECM). Among the various technique for the fabrication of nanofibrous scaffolds, the electrospinning method is the most promising and versatile process, mainly due to its ability to create nanofibers with the physical dimensions similar to the fibrillar ECM, processing versatility to a wide range of polymers, potential to include ceramic nanoparticles, and simple operation at low cost (Sadat-Shojai and Moghaddas 2020; Sadat-Shojai and Moghaddas 2021). The method uses an externally applied electric force to draw charged threads of polymer solutions as thin jets from a capillary tube towards a collector (Sadat-Shojai and Moghaddas 2021; Turnbull et al. 2018). The first step in electrospinning process is preparation of the polymer solution with an appropriate viscosity and surface tension. There have already been numerous studies on electrospun nanofibers from various natural polymers (Angel et al. 2020; Bombin et al. 2020; Hooshmand-Ardakani et al. 2020; Zarei et al. 2021); however, since naturally occurring cellulose is insoluble in most organic solvents owing to its high crystallinity enhanced by tremendous hydrogen bonding network, most of the researchers have focused on cellulose derivatives and only few attempts have been made for direct electrospinning of dissolving cellulose. On the other hand, electrospinning of cellulose derived from plants in conjugation with HA nanoparticles has rarely been reported, probably because it may be difficult to prepare a convenient solution/dispersion with high solution concentration in terms of cellulose and high dispersion stability in terms of HA nanoparticles.

Thus, the aim of the present study was to fabricate nanofibrous cellulose/HA mats with the electrospinning process at some new processing conditions with the aid of design of experiments (DOE) approach. To our knowledge, no electrospinning study has been conducted using DOE approach to explore the influence of fabrication process on properties of cellulose-based scaffold. Banana pseudo-stem (BPS) by-product generated in banana is a kind of raw materials which primarily consists of cellulose, hemicellulose and lignin, and hence we first attempt to extract α-cellulose from BPS by a

liquefaction method, followed by physical characterization of the producing bleached liquefied residue (BLR). The optimal conditions of electrospinning for BLR in trifluoroacetic acid (TFA)/1,2-dichloroethane (DCE) solvent mixture was then determined using DOE and analysis of the obtained responses. Nanofibrous cellulose scaffolds having different concentrations of HA nanoparticles were also fabricated under optimized conditions to determine the effect of HA bioceramics on physical, biological and mechanical properties of the cellulose-based scaffolds.

Experimental

Materials

BPS (collected from Fars, Shiraz, Iran) was washed and dried at 100°C, followed by milling to obtain a fine and homogeneous powder. Polyethylene glycol 400 (PEG 400), glycerol, sulfuric acid (98%) and sodium chlorite were purchased from Merck and used for extraction of cellulose from BPS. $Ca(NO_3)_2.4H_2O$ (Merck) as the calcium ion source, $(NH_4)_2HPO_4$ (Merck) as the phosphate ion source, and NH_4OH (Merck) as the pH controller were used for the preparation of HA nanoparticles. Merck-grade NaCl, $NaHCO_3$, KCl, $K_2HPO_4.3H_2O$, $MgCl_2.6H_2O$, $CaCl_2$, Na_2SO_4, tris(hydroxymethyl)aminomethane ($(CH_2OH)_3CNH_2$,), and HCl were used for preparation of simulated body fluid (SBF). Phosphate buffered saline (PBS) was purchased from Invitrogen Corporation. Solvents including TFA, DCE, and dimethylacetamide (DMAc) were come from Sigma and used as received. All reagents and chemicals were of reagent grade and were used without further purification.

Extraction of cellulose from BPS

Extraction of cellulose from BPS was conducted according to a procedure described elsewhere, with some modifications (Meng et al. 2019). In brief, to remove most hemicelluloses and some lignin from BPS by liquefaction method, 25 g of mixed solvents (PEG 400 : glycerol = 4:1, w/w) and 0.49 g of sulfuric acid as a catalyst were first added to a glass flask and preheated to 150°C. 5 g of BPS was then added to the liquid to start the reaction. After constant stirring and refluxing for 90 min, the flask was quickly immersed into an ice-bath to quench the reaction. The resulting black precipitate was diluted with ethanol. Thereafter, the liquefied residue (LR) was collected by filtration and dried at 100°C. The bleaching process of LR was carried out by the sodium chlorite method. For this, LR was treated by acidified sodium chlorite solution (6 wt%, pH 4~4.5 by acetic acid) at 75°C for 1h to remove residual lignin. This treatment was repeated for at least 3~5 times until the obtaining residue became colorless. The mixture was cooled and rinsed thoroughly with the deionized water, followed by freeze drying to obtain the final bleached LR (BLR). The chemical structure of BPS, LR and BLR was studied using Fourier transform infrared spectroscopy (FTIR; 8300, Shimadzu, Japan) according to the KBr technique. Phase composition of the prepared BLR was analyzed using a X-ray diffractometer (XRD, D8 advanced, Bruker, Germany) with CuKα (λ = 1.54187 Å) incident radiation over the 2θ range of 10–50° at room temperature with a step size of 0.05°. The relative crystallinity index (Cr.I.) of the product was determined following Eq. 1 (Jasiukaitytė et al. 2009; Segal et al. 1959):

$$\mathrm{Cr.\,I.\,(\%)} = \frac{\mathrm{I_{200}} - \mathrm{I_{am}}}{\mathrm{I_{200}}} \times 100$$

1

where I_{200} is maximum intensity of the diffraction from the 2 0 0 lattice plane at 2θ of 22°, and I_{am} represents the diffraction intensity of the amorphous background scatter corresponding to the intensity of the minimum between 1 1 0 peak and 2 0 0 peak at 2θ of about 18° (Segal et al. 1959). Moreover, the average thickness of cellulose crystallites was estimated by using Scherrer's Eq. 2 (Jasiukaitytė et al. 2009):

$$\mathrm{D_{hkl}} = \frac{\mathrm{K}\lambda}{\beta_{1/2}\cos\theta}$$

2

where D_{hkl} is the crystallite dimension in the direction normal to the h k l of lattice planes, K is the correction factor equal to 0.9, λ is the X-ray wavelength (0.154187 nm), θ is the diffraction angle and $\beta_{1/2}$ is the peak width at half maximum intensity. In this study, the crystallite size was estimated perpendicular to the 2 0 0 plane where $\beta_{1/2}$ was determined as 0.27 rad. Molecular weight (MW) of BLR sample was determined by the capillary viscometry method using the Ubbelohde U-tube viscometer. For this, BLR was dissolved in DMAc/9% LiCl solvent at 25°C and the MW was estimated using Mark-Houwink equation which relates the MW of the polymer to the intrinsic viscosity [□] (Chuah et al. 2001):

$$[\square] = \mathrm{KM^a}$$

3

where, K and a are Mark-Houwink constants, which in DMAc/LiCl solvent system at 25°C, are equal to 0.001278 mL/g and 1.19, respectively (McCormick et al. 1985).

Synthesis of HA nanoparticles

HA nanoparticles were synthesized in-house according to our previously reported procedure (Sadat-Shojai and Moghaddas 2020). In brief, a solution of $(NH_4)_2HPO_4$ (0.15 M) was added into a solution of $Ca(NO_3)_2.4H_2O$ (0.15 M) at a constant rate and continuous stirring, while molar ratio of calcium ions to phosphate ions was kept at 1.67. During the reaction, pH was adjusted at 10 using a diluted NH_4OH solution. The solution containing particles was subsequently aged in a sealed container at 90°C for 60 h. Finally, the HA nanoparticles were separated and washed by a mixture of ethanol and deionized water. Chemical structure and phase composition of powder was examined using FTIR and XRD respectively. Moreover, crystalline phase and crystallite size of particles were determined by using the XRD spectrum following the methods described in the literature (Pang and Bao 2003; Reiche et al. 2002). The morphology of the powder was investigated using scanning electron microscopy (SEM, Vega3, TESCAN, Czech Republic) and transmission electron microscopy (TEM, CM10, Philips, Netherlands). SBF solution with an ionic concentrations similar to those of human blood plasma was adopted to survey the

bioactivity of the as-synthesized nanoparticles. For this, SBF solution was first prepared according to the protocol described elsewhere (Kokubo and Takadama 2006), and the in vitro bioactivity was then assessed by soaking the powder in the SBF for 30 days at 37°C, while the solution was refreshed every three days. The powder sample was subsequently filtered and washed thoroughly with deionized water before analysis with SEM.

Taguchi experimental design approach

Statistical DOE-based methods are one of the most useful tools to optimize the process parameters and to extract as much information as possible from fewer experiments. Indeed, this approach aims to understand the impact of several parameters on selective responses while minimizing the number of trials (Gadomska-Gajadhur et al. 2018; Sadat-Shojai and Ghadiri-Ghalenazeri 2020; Smiciklas et al. 2005). Among the possible DOE approaches, the Taguchi method based on an orthogonal array has recently received great attention as it can obtain the optimum conditions through a very limited number of tests. Furthermore, this method can simply identify those input variables which have the major impact on the selected response (Sadat-Shojai and Ghadiri-Ghalenazeri 2020). As shown in Table 1, four process variables, which are well-known to be important electrospinning parameters, with three levels for each were selected in the current study and a Taguchi method based on an L_9 orthogonal array was employed to examine their effects on the objective functions, i.e. average diameter of cellulose nanofibers and average area of splashing during the electrospinning. According to Table 1, the total number of required trials was only 9 as opposed to 81 for a full factorial design. The present study is the first study investigating the optimum electrospinning conditions for the fabrication of cellulose-based nanofibers. Here, Taguchi's S/N ratios along with relevant mean plots was automatically obtained using the software "STATISTICA 12.0®". Finally, the fabrication of cellulose nanofibers with the smallest diameter and the best uniformity (i.e., the lowest splashing) was attempted by applying the best level of each electrospinning variable.

Electrospinning of cellulose nanofibers

The electrospinning was performed using a labscale electrospinning unit (Nanoazma, Iran) at room temperature and relative humidity of ~30%. For this, cellulose solutions with different concentrations (according to Table 1) were prepared by stirring the appropriate amounts of BLR in mixed TFA/DCE solvent (7:3, v/v) for two days at room temperature. The obtaining viscous and homogeneous solution was then transferred to a syringe capped with a blunt-ended needle. A metallic electrode plate wrapped with aluminum foil was used as a collector while the nozzle to collector distance (i.e., working distance, WD) was fixed according to the values in Table 1. High voltage according to Table 1 was applied between the needle and the electrode plate and the cellulose solution flows from the needle with a predetermined flow rate (Table 1) to collect the nanofibers on the aluminum foil. Both the flow late and the applied electric voltage were tried to precisely control to keep stable cone-like structure of the cellulose solution on the tip of the nozzle during electrospinning process. To estimate the mean fiber diameter, the morphology of nanofibers was studied using SEM, followed by diameter measurement of 100 randomly

selected individual fibers using Image J software. In addition, the average area of splashing was estimated through image analysis of around 20 splashed particulates from four images.

Electrospinning of cellulose/HA nanofibers

To prepare cellulose/HA mixture for electrospinning, cellulose was first dissolved at the optimum concentration in TFA/DCE solvent according to the procedure described in previous section. HA nanoparticles was then dispersed in the resulting solution through 5 min sonication in an ultrasonic bath. The mixed solution/dispersion with HA concentration varying from 0–20% (w/w, with respect to the cellulose) was subsequently electrospun under optimum conditions determined through the statistical DOE approach. The obtaining nanofibrous structures containing 0, 10, and 20 wt.% HA nanoparticles were denoted as C-HA0, C-HA10, and C-HA20 respectively. To evaluate the colloidal stability of HA nanoparticles in the electrospinning solution, a sedimentation study was performed through a typical solution/dispersion of cellulose with HA concentration of 10%. For this, the nanoparticles were dispersed in cellulose solution using the ultrasonic bath and the sedimentation behavior was immediately monitored for 6 h.

The morphology of the nanofibrous composites was evaluated using SEM, while the dispersion of HA particles inside the nanofibers was assayed using an energy dispersive X-ray analyzer (EDX, QX2, Rontec) which was coupled with the SEM microscopy. To estimate the porosity, the apparent density of a 2 cm × 2 cm piece of the fibrous mat was first determined using Eq. 4 (Ma et al. 2005):

$$\mathrm{apparentdensity}(\mathrm{g}/\mathrm{cm}^3) = \frac{\mathrm{matmass}(\mathrm{mg}) \times 10}{\mathrm{matthikness}(\mu\mathrm{m}) \times \mathrm{matarea}\left(\mathrm{cm}^2\right)}$$

4

Then, the porosity was calculated according to Eq. 5 (Ma et al. 2005):

$$\mathrm{matporosity}(\backslash\%) = \left(1 - \frac{\mathrm{apparentdensity}(\mathrm{g}/\mathrm{cm}^3)}{\mathrm{bulkdensityoffilm}(\mathrm{g}/\mathrm{cm}^3)}\right) \times 100$$

5

where the bulk density was determined through density measurement of a non-porous casted film obtained from solution casting of a 2 cm × 2 cm piece of the fibrous mat dissolved in DMAc/LiCl solvent at room temperature. To investigate the mechanical strength of nanocomposites, uniaxial tensile tests were performed by using a universal testing machine (Z020, Zwick/Roell, Germany) equipped with a 20 N load cell. Rectangular strips of ~5 mm × 20 mm × 0.1 mm were cut from each nanofibrous mat and the samples were placed between the grips of the machine and pulled apart in the longitudinal direction at a constant crosshead speed of 1.0 mm/min. The tensile strength was subsequently determined according to the maximum stress detected from the stress–strain curves, while the elastic modulus was calculated from the first linear slop of the curves. Four measurements were conducted for each sample and the

obtained values were reported as mean ± standard deviation (SD). The water contact angle of fibrous surface was estimated to determine the relative hydrophilicity of the mats. For this, 5.0 µL of deionized water was placed on the mat and the water droplet image was immediately captured, from which the contact angle was estimated and reported as mean ± SD of three measurements. To evaluate the biodegradability, samples in triplicate were cut into square pieces, weighed, and then immersed in PBS solution at 37°C. The samples were subsequently removed from the PBS solution, washed four times with deionized water, dried and finally weighed, to assess the weight loss due to cellulose degradation. The degradation was evaluated weekly over the predicted period of time. The in vitro bioactivity was studied by soaking nanofibrous mat containing 20 wt.% HA in SBF solution at 37°C for 30 days. The SBF solution was refreshed every three days. Finally, the mat was removed from the solution, washed with deionized water, and dried before evaluation by SEM.

Statistical analysis

All data were presented as representative images or as means ± SD. The generated data were compared using both the Tukey's test and one-way ANOVA. Differences between the experimental groups were then considered statistically significant only when $p < 0.05$.

Results And Discussion

Cellulose

Cellulose occurs in almost pure form in cotton fibers; however, in plants, it is found in conjugation with other raw materials, such as lignin and hemicelluloses (Kalia et al. 2011; Meng et al. 2019). In the current study, cellulose was therefore isolated from BPS using the liquefaction method followed by the bleaching process. In this strategy, impurities, including lignin and hemicelluloses can be solubilized by liquefaction, while the residual lignin can be removed using the bleaching process (Meng et al. 2019). The resulting BLR was then used as the polymeric material for fabrication of cellulose/HA nanofibers. The overall macroscopic appearance for the BPS after two steps of treatment is shown in Fig. 1a. According to the figure, the milled light brown BPS powder changed to brownish-black residue (i.e., LR) as a result of the creation of some chromophore during the liquefaction treatment. However, the bleached component (i.e., BLR) appears as a white powder, confirming that hemicellulose, lignin and other non-cellulosic substances were completely removed by the extraction process; accordingly, the final product is suggested to be almost pure cellulosic material. Fig. 1b shows FTIR spectra of BPS, LR and BLR to compare the change in chemical structure resulting from this purification process. All spectra exhibited the typical characteristic bands of cellulose, e.g. 3100–3500 cm^{-1} (OH stretching), 2900 cm^{-1} (CH stretching), 1450 cm^{-1} (CH_2 bending), 1305 cm^{-1} (CH asymmetric deformations) and 1035–1095 cm^{-1} (CO stretching) (Li et al. 2015; Meng et al. 2019). In contrast, no significant absorption bands at 1735 and 1244 cm^{-1} due to C=O stretching vibrations of lignin and hemicellulose and C-O-C vibrations of aromatic ether linkages in lignin can be detected in BLR spectrum, indicating that lignin and hemicellulose content

can be relatively removed after the liquefaction and bleaching processes. Therefore, the results indicated that the chemical structure of cellulose chains remains unchanged following the conducted treatments.

To examine the crystalline structure of the produced cellulose, XRD analysis was used as depicted in Fig. 1c. Indeed, its linearity along with hydrogen bonding interactions and van der Waals forces between adjacent molecules can induce a closely packed crystalline structure in cellulose (Zhang et al. 2004). According to the diffraction pattern of BLR, two peaks at around $2\theta = 22^{\circ}$ and 15.3°, corresponding to the 2 0 0 and 1 1 0 plane positions, can be detected confirming a typical crystalline polymorph of cellulose I (French 2014; Li et al. 2015; Meng et al. 2019). The Cr.I. and thickness of cellulose crystallites determined respectively using Eqs. 1 and 2 were 51.8% and 5.22 nm respectively, which were very close to the values reported in the literature (Manimaran et al. 2020; Pelissari et al. 2014). While, the Cr.I. for naturally produced BPS has been reported around 8.7%. (Meng et al. 2019), the higher degree of crystallinity of BLR compared to BPS can be attributed to the progressive removal of amorphous hemicellulose, lignin and other non-cellulosic contents due to the successive liquefaction and bleaching treatments. To study whether the producing cellulose was suitable for the electrospinning, we also assessed the MW of BLR with the well-known Mark-Houwink equation which relates the MW of cellulose to [] (Eq. 3). While, many characteristics of cellulose depend on its chain length or the degree of polymerization, MW of the extracted cellulose from various plant sources are reported between 1.0×10^4 and 8.0×10^5 (Immergut et al. 2953). In a typical electrospinning process, higher molecular weights of the polymer (i.e., larger chains) favors uniform fiber formation. On the other hand, number of beads in the fiber structure decreases with increasing MW (Gupta et al. 2005; Rezaei et al. 2015). According to our viscometry and Eq. 3, the estimated MW of the produced cellulose was around 3.0×10^5 which is acceptable for a plant-origin cellulosic polymer.

HA nanoparticles

Nanosized HA particles have long been applied as reinforcing agent in polymeric nanocomposites, as they can significantly enhance their biocompatibility, bioactivity, osteoconductivity and mechanical strength (Sadat-Shojai 2015). In the current study, the as-synthesized HA nanoparticles were characterized in terms of their morphology, chemical structure, and bioactivity. The colloidal stability of HA in BLR solution was also investigated. According to XRD analysis (Fig. 2b) and the ICDD standard card no. 00-09-0432, the as-synthesized powder was relatively pure HA phase with a hexagonal crystal system. From the XRD data, the crystallinity index and the crystallite size (for isolated peak assigned to 2 0 0 plane) was 0.80 and 43 nm, respectively. Moreover, the IR spectrum depicted in Fig. 2b confirmed the chemical composition of the precipitate in accordance with the formula of HA (i.e., $Ca_{10}(PO_4)_6(OH)_2$) (Pang and Bao 2003; Sadat-Shojai and Moghaddas 2020). Fig. 2c shows SEM and TEM micrographs of the powder, indicating that prepared particles were relatively irregular in shape with an average grain size less than 70 nm. Since the purpose of this study was to fabricate bone scaffolds, it was necessary to examine the in vitro bioactive properties of the as-synthesized particles. Fig. 2d shows the SEM of particles after 30 days immersion in SBF at 37°C, indicating generation of a flake-like microstructure as a result of nucleation of new minerals on the surface of nanoparticles. Accordingly, the HA powder

prepared here have relatively high bioactivity and hence may be a good candidate as reinforcing agent in polymer scaffolds. A colloidal stability study which is usually considered as the sedimentation behavior of particles was performed to investigate the duration of HA dispersion in BLR/TFA solution. According to the results (Fig. 3), there is not any significant aggregation and/or precipitation of nanoparticles until 1 h after the sonication. Indeed, during one hour of monitoring, the suspension containing HA nanoparticles remained completely turbid. As the electrospinning of cellulosic nanofibers containing particles takes a maximum of 1 h, these results can guarantee that nanoparticles can remain stable in the organic phase during the process. However, as indicated in Fig. 3, for longer times (up to 6 hours) some nanoparticles begin to precipitate and some others dissolve in the acidic solution, indicating that the as-synthesized powder cannot remain stable for long periods.

Analysis of the electrospinning experiments

The DOE is known to be a powerful tool for achieving specific goals, simultaneously examining several control factors, and systematically evaluating empirical data (Gadomska-Gajadhur et al. 2018; Smiciklas et al. 2005). Among the possible DOE methods, Taguchi design, as an orthogonal array method, can optimize several processing variables and extract large quantitative information from just a few experimental trials. In addition, this method efficiently identifies those input variables which have the major impact on the selected response (Sadat-Shojai and Ghadiri-Ghalenazeri 2020). Therefore, in the fabrication of cellulosic nanofibers using electrospinning method, a Taguchi experimental design based on an L_9 orthogonal array seems to be an appropriate approach to optimize the processing variables and to study their influence on the fiber diameter and degree of splashing. For this, among the factors that may influence the electrospun fibers, solution concentration, voltage, flow rate and WD were evaluated using a three-level Taguchi series experimental design approach. In this strategy, the response of the fiber diameter and degree of splashing were determined by image analysis of SEM micrographs.

It is well-known that critical characteristics of electrospun fibers, such as mechanical strength and toxicity to cells depend strongly upon their microstructure, mainly their morphology, orientation, uniformity, and fiber diameter (Bombin et al. 2020; Hooshmand-Ardakani et al. 2020; Sadat-Shojai and Moghaddas 2020; Sadat-Shojai and Moghaddas 2021; Zarei et al. 2021). However, when one considers the nanofibers, their dimensions seemed to be highlighted more than other characteristics. Figs. 4 and 5a show SEM photomicrographs and diagram of estimated dimensions of the electrospun nanofibers, respectively. According to the SEM observations, two types of morphologies were formed depending on the processing conditions. As seen in SEM images of run no. 1 to run no. 5, a non-uniform fibrous structure with a large amount of splashing was obtained through electrospinning at low solution concentrations (i.e., 1 and 1.4 wt.%). However, Fig. 4 shows, while an increase in solution concentrations to 1.6 wt.% with a higher applied voltage of 25 kV (i.e., run no. 8) resulted in a uniform structure, a further increase in voltage to 30 kV with the minimum working distance of 10 cm (i.e., run no. 9) yielded a very uniform and interesting nanofibrous mat. According to Fig. 5a, among the studied variables, the high influence of the solution concentration is evident by the significant increase in fiber diameter with increasing the solution concentration. Since fibers are generated by evaporation of the solution jet, the diameter of the nanofibers

largely depends on the size of the jet as well as the concentration of polymer in the solution jet. Several researchers have suggested that the higher the viscosity of the electrospinning solution, the larger the diameter of the generated fibers (Nezarati et al. 2013; Zeng et al. 2003). Accordingly, the reason behind the increase in the fiber diameter, as shown, is the increase in solution viscosity and the difficulty of pulling the jet at higher concentrations. Moreover, at higher cellulose concentrations, the amount of solvent in the solution jet is less and hence the solvent can evaporate faster. Therefore, with a more concentrated solution, drawing the jet becomes more difficult and dry fibers with larger diameters are generated on the collector. Although smaller diameters for nanofibers may be preferred due to their higher similarity to the natural ECM, as shown in Fig. 5b, the amount of solution splashing (i.e., droplet formation) decreases significantly with increasing fiber diameter from run no. 1 to run no. 9. Indeed, for low-viscosity solution the polymer chains are not entangled and jet is unstable and breaks up into droplets; accordingly to achieve fibers with a lower splashing, solutions with higher concentrations should be used.

A graphical display of the level effect of each electrospinning variable is given in the mean plots in Fig. 5c, in which analyses of the magnitude and the importance of each input factor's effect are shown. In addition, Table 2 indicates the maximum S/N ratios generated at the optimum level. Again, according to Fig. 5c and Table 2, the cellulose concentration of the electrospinning solution has the greatest effect on the selected responses. Moreover, while the applied voltage during the electrospinning process can also affect the fiber diameter and amount of splashing, based on the S/N ratios, the flow rate and working distance have the lowest importance among the studied factors. From these results, the optimum level for each electrospinning parameter was confirmed as: solution concentration of 1.6 wt.%; applied voltage of 30 kV; flow rate of 0.5 mL/h and WD of 10 cm.

Cellulose/HA nanofibers

Although electrospun nanofibers from native cellulose have been previously reported, very few studies, to the best of our knowledge, were focused on development of electrospun cellulose nanofibers containing HA nanoparticles. Moreover, a comprehensive characterization of cellulose nanofibers have rarely been reported before. However, it is expected that stiff and bioactive HA nanoparticles would remarkably influence the structural, mechanical and biological properties of the electrospun cellulosic mats. The morphological characteristics of the as-spun composite fibers were examined using SEM as shown in Fig. 6a. As can be seen, due to the optimization of the electrospinning conditions, the created nanofibrous structures are uniform with minimal bead and splashing defects. Indeed, the absence of beads and splashing droplets can increase surface area-to-volume ratio of the fibers, which in turn increases the contact area between the fibers and the living cells. On the other hand, according to SEM observations, there is not any significant particle agglomeration and/or aggregation in C-HA10 and C-HA20 samples, suggesting that HA nanoparticles could be homogeneously embedded in the cellulose nanofibers at the expected concentrations. The complete encapsulation of nanoparticles may result from significantly larger diameter of the nanofibers compared with that of the nanoparticles. To further confirm the homogeneous distribution and dispersion of filler inside the fibrous matrix, EDX-mapping of

nanoparticles for C-HA20 sample was also carried out as shown in Fig. 6b. Again, the results clearly suggested that HA nanoparticles were well encapsulated and evenly dispersed inside the whole fibrous mat.

Diameter of the as-spun fibers were determined from SEM images and the results were summarized in Fig. 6c. According to the results, the diameters of the nanofibers decreased non-significantly with the addition of nanoparticles. The observed decrease in the fiber diameter with increasing concentration of filler may result from the fact that reduction of viscosity of the solution jet near the collector can occur due to the lower fraction of the polymer. Interconnected porosity is another essential requirement for artificial tissue engineering scaffolds. Indeed, scaffolds should mimic the native ECM in terms of porosity to allow proper cell and nutrient migration (Bombin et al. 2020; Sadat-Shojai and Arvaneh 2021; Zarei et al. 2021). The porosity degrees calculated using Eq. 5 were summarized in Fig. 6d. According to the figure, there was a non-significant increase from 61–69% in porosity with increasing HA concentration, suggesting that the degree of porosity may slightly be controlled with the filler concentration, although more investigations is needed to determine the reason behind this effect.

An important characteristic to be considered for bone scaffolds is mechanical strength. Generally, the mechanical strength of an electrospun fibrous scaffold is controlled by several parameters, including intrinsic characteristics of the polymer (mainly its molecular weight), degree of porosity, average diameter size of fibers, and presence of defects (Han et al. 2020; Tarus et al. 2016). Fig. 7a illustrates the representative stress-strain curves of C-HA0, C-HA10 and C-HA20 fibrous samples. From these curves and their extracted data, the elastic moduli and the tensile strengths of the samples were determined as shown in Figs. 7b and 7c respectively. According to the results (Fig. 7b), the samples containing HA have a higher elastic modulus with respect to the sample C-HA0, owing to the incorporation of HA as a stiff filler. Moreover, the amount of modulus increased significantly with increasing the filler concentration. The obtained results were in agreement with the results of our previous studies in which mechanical strength of various polymers was a function of the filler content (Sadat-Shojai 2015; Sadat-Shojai and Moghaddas 2020; Sadat-Shojai and Moghaddas 2021). In fact, when the high modulus HA reinforcement was conjugated with the lower modulus cellulose, applied stress transfers from the polymeric matrix to the stiff filler, leading to an increase in the average modulus. The addition of high-modulus HA increased the tensile strength of the cellulose as well. As shown in Fig. 7c, sample C-HA20 has the highest tensile strength, which indicates a direct relationship between the addition of HA and tensile strength.

Fabricating electrospun mat with satisfactory biological properties is one of the great challenges in attempting to design bone scaffolds. In the current study, to investigate the biological properties of the fabricated nanocomposites, their degree of wetting was first determined by using contact angle measurement. Contact angle, in turns, depends on several parameters including hydrophobicity of nanocomposite, surface roughness and degree of porosity (Gu et al. 2016; Sadat-Shojai and Moghaddas 2020). According to the results (Fig. 8a), the nanocomposite containing the highest amount of filler (i.e., C-HA20) exhibited a water contact angle of 91 ± 5.7 $^{\circ}$, which was significantly smaller than control (C-HA0, 112 ± 5.6 $^{\circ}$). The greater wettability of C-HA20 should obviously be attributed to the incorporation of

HA particles as a hydrophilic filler. Biodegradability analysis of biomaterials provides a useful tool to assay their suitability for tissue engineering applications. Indeed, scaffolds should be degradable naturally over the time to permit new tissue to form. The weight loss of the C-HA20 sample with regard to degradation time is shown in Fig. 8b, suggesting that around 5% weight loss can occur after six weeks incubation in PBS at 37°C. It is noticeable that two other samples including C-HA10 and C-HA0 did not show a significant weight loss until the sixth week in vitro, indicating that the prepared cellulose is hardly degradable in aqueous solutions with neutral pH and the absence of enzymes. On the other hand, the relative biodegradability of C-HA20 was due to its high concentration of incorporated HA, which can increase the water uptake and hence adjust its degradation rate. The bioactivity of fibrous filled nanocomposite with the highest HA concentration (i.e., C-HA20) was evaluated after soaking in SBF solution for 30 days under physiological conditions. Fig. 8c shows an interesting apatite particles aggregates forming a flake-like structure deposit on the surface of the nanofibers. This is surprising because according to the morphological studies (Fig. 6a), almost all HA nanoparticles were encapsulated inside the fibers and therefore there was no direct contact between the nanoparticles and the SBF liquid. Overall, these results confirmed that the fabricated scaffold has bioactivity and has the ability to form a new apatite phase on its surfaces, which in turn leads to a direct bonding to the living bone after its implantation in the body.

Conclusions

In summary, highly accessible cellulose type I crystals with MW of 3.0×10^5 were extracted from BPS by a liquefaction method followed by bleaching treatment. The extracted native cellulose was then tried to electrospun in TFA/DCE to determine how a systematic approach based on a Taguchi L_9 orthogonal array can be used to fabricate a defect-free fibrous mat. The results showed that the solution concentration has the greatest effect on the morphology of the electrospun mat. Moreover, while the applied voltage during the electrospinning process can also affect the fiber diameter and amount of splashing, based on the S/N ratios, the flow rate and WD have the lowest importance among the studied factors. The electrospun cellulose/HA mats with HA concentration varying from 0–20% were subsequently fabricated under the optimum conditions. SEM micrographs and EDX-mapping revealed that obtained fibrous mats have a uniform fiber texture without any significant bead, splashing or particle agglomeration. The results also suggested that HA nanoparticles were well encapsulated and evenly dispersed inside the whole fibrous mat. On the other hand, incorporation of HA nanoparticles into the cellulose nanofibers resulted in a change in the fiber diameter and degree of porosity, although both the effects were non-significant. According to the mechanical results, the samples containing the highest concentration of HA (i.e., C-HA20) have a significantly highest elastic modulus and tensile strength, owing to the incorporation of HA as a stiff filler. While C-HA20 showed a relatively low biodegradability, a surprising result was an interesting morphological transformation from smooth nanofibers into a flake-like structure after 30 days incubation in SBF, which confirmed the high bioactivity of the nanofibers. Accordingly, the fibrous scaffolds developed in this study demonstrated excellent potential for the application in bone tissue engineering.

Declarations

Acknowledgement

The authors would like to acknowledge funding from Shiraz University (No. 99GCB1M256440).

Conflict of interest

The authors declare that they have no conflict of interest.

Ethical standards

This study was conducted following Compliance with Ethical Standards, and it did not involve human participants, animals, and potential conflicts of interest.

References

1. Angel N, Guo L, Yan F et al (2020) Effect of processing parameters on the electrospinning of cellulose acetate studied by response surface methodology. J Agric Food Res 2:100015. https://doi.org/10.1016/j.jafr.2019.100015
2. Bombin ADJ, Dunne NJ, McCarthy HO (2020) Electrospinning of natural polymers for the production of nanofibres for wound healing applications. Mater Sci Eng C 114:110994. https://doi.org/10.1016/j.msec.2020.110994
3. Chuah H, Lin-Vien D, Soni U (2001) Poly (trimethylene terephthalate) molecular weight and Mark–Houwink equation. Polymer 42:7137–7139. https://doi.org/10.1016/S0032-3861(01)00043-X
4. French AD (2014) Idealized powder diffraction patterns for cellulose polymorphs. Cellulose 21:885–896. https://doi.org/10.1007/s10570-013-0030-4
5. Gadomska-Gajadhur A, Wrzecionek M, Matyszczak G et al (2018) Optimization of Poly (glycerol sebacate) Synthesis for Biomedical Purposes with the Design of Experiments. Org Process Res Dev 22:1793–1800. https://doi.org/10.1021/acs.oprd.8b00306
6. Gu H, Wang C, Gong S et al (2016) Investigation on contact angle measurement methods and wettability transition of porous surfaces. Surf Coat Tech 292:72–77. https://doi.org/10.1016/j.surfcoat.2016.03.014
7. Gupta P, Elkins C, Long TE, Wilkes GL (2005) Electrospinning of linear homopolymers of poly (methyl methacrylate): exploring relationships between fiber formation, viscosity, molecular weight and concentration in a good solvent. Polymer 46:4799–4810. https://doi.org/10.1016/j.polymer.2005.04.021
8. Han Y, Xu Y, Zhang S et al (2020) Progress of improving mechanical strength of electrospun nanofibrous membranes. Macromol Mater Eng 305:2000230.

https://doi.org/10.1002/mame.202000230

9. Hooshmand-Ardakani A, Talaei-Khozani T, Sadat-Shojai M et al (2020) In Vitro Characterization of Multilamellar Fibers with Uniaxially Oriented Electrospun Type I Collagen Scaffolds. Adv Mater Sci Eng 2020:1–13. https://doi.org/10.1155/2020/4084317
10. Immergut E, Ranby B, Mark H (1953) Recent work on molecular weight of cellulose. Ind Eng Chem 45:2483–2490. https://doi.org/10.1021/ie50527a036
11. Jasiukaitytė E, Kunaver M, Strlič M (2009) Cellulose liquefaction in acidified ethylene glycol. Cellulose 16:393–405. https://doi.org/10.1007/s10570-009-9288-y
12. Kalia S, Dufresne A, Cherian BM et al (2011) Cellulose-Based Bio- and Nanocomposites. A Review Int J Polym Sci 2011:837875. https://doi.org/10.1155/2011/837875
13. Kokubo T, Takadama H (2006) How useful is SBF in predicting in vivo bone bioactivity? Biomaterials 27:2907–2915. https://doi.org/10.1016/j.biomaterials.2006.01.017
14. Li W, Zhang Y, Li J et al (2015) Characterization of cellulose from banana pseudo-stem by heterogeneous liquefaction. Carbohydr Polym 132:513–519. https://doi.org/10.1016/j.carbpol.2015.06.066
15. Ma Z, Kotaki M, Yong T et al (2005) Surface engineering of electrospun polyethylene terephthalate (PET) nanofibers towards development of a new material for blood vessel engineering. Biomaterials 26:2527–2536. https://doi.org/10.1016/j.biomaterials.2004.07.026
16. Manimaran P, Pillai GP, Vignesh V, Prithiviraj M (2020) Characterization of natural cellulosic fibers from Nendran Banana Peduncle plants. Int J Biol Macromol 162:1807–1815. https://doi.org/10.1016/j.ijbiomac.2020.08.111
17. McCormick CL, Callais PA, Hutchinson BH Jr (1985) Solution studies of cellulose in lithium chloride and N, N-dimethylacetamide. Macromolecules 18:2394–2401. https://doi.org/10.1021/ma00154a010
18. Meng F, Wang G, Du X et al (2019) Extraction and characterization of cellulose nanofibers and nanocrystals from liquefied banana pseudo-stem residue. Compos B Eng 160:341–347. https://doi.org/10.1016/j.compositesb.2018.08.048
19. Nezarati RM, Eifert MB, Cosgriff-Hernandez E (2013) Effects of humidity and solution viscosity on electrospun fiber morphology. Tissue Eng Part C Methods 19:810–819. https://doi.org/10.1089/ten.TEC.2012.0671
20. Pang Y, Bao X (2003) Influence of temperature, ripening time and calcination on the morphology and crystallinity of hydroxyapatite nanoparticles. J Eur Ceram Soc 23:1697–1704. https://doi.org/10.1016/S0955-2219(02)00413-2
21. Pelissari FM, Amaral Sobral PJ, Menegalli FC (2014) Isolation and characterization of cellulose nanofibers from banana peels. Cellulose 21:417–432. https://doi.org/10.1007/s10570-013-0138-6
22. Perić Kačarević Ž, Rider P, Alkildani S et al (2020) An introduction to bone tissue engineering. Int J Artif Organs 43:69–86. https://doi.org/10.1177%2F0391398819876286

23. Reiche I, Vignaud C, Menu M (2002) The crystallinity of ancient bone and dentine: new insights by transmission electron microscopy. Archaeometry 44:447–459. https://doi.org/10.1111/1475-4754.00077
24. Rezaei A, Nasirpour A, Fathi M (2015) Application of cellulosic nanofibers in food science using electrospinning and its potential risk. Compr Rev Food Sci Food Saf 14:269–284. https://doi.org/10.1111/1541-4337.12128
25. Sadat-Shojai M (2015) Calcium phosphate reinforced polyester nanocomposites for bone regeneration applications. In: Depan D (ed) Biodegradable polymeric nanocomposites: advances in biomedical applications, 1st edn. Taylor & Francis Publisher (CRC Press), USA, pp 1–34
26. Sadat-Shojai M (2018) Controlled pattern of cell growth in modulated protein nanocomplexes: regulating cells spreading in three dimensions. Mater Today 21:686–688. http://dx.doi.org/10.1016/j.mattod.2018.06.003
27. Sadat-Shojai M, Arvaneh AR (2021) Biodegradable aliphatic polyesters for application in tissue engineering. Iran J Polym Sci Technol, Accepted (In press)
28. Sadat-Shojai M, Ghadiri-Ghalenazeri S (2020) A modular strategy for fabrication of responsive nanocomposites using functionalized oligocaprolactones and hydroxyapatite nanoparticles. New J Chem 44:20155–20166. https://doi.org/10.1039/D0NJ03453C
29. Sadat-Shojai M, Moghaddas H (2020) How geometry, size, and surface properties of tailor-made particles control the efficiency of poly (3-hydroxybutyrate-co-3-hydroxyvalerate) /hydroxyapatite nanocomposites. J Appl Polym Sci 137:49810. https://doi.org/10.1002/app.49810
30. Sadat-Shojai M, Moghaddas H (2021) Modulated Composite Nanofibers with Enhanced Structural Stability for Promotion of Hard Tissue Healing. Iran J Sci Technol Trans A Sci 45:529–537. https://doi.org/10.1007/s40995-020-01016-w
31. Sato K (2007) Mechanism of hydroxyapatite mineralization in biological systems. J Ceram Soc Japan 115:124–130. https://doi.org/10.2109/jcersj.115.124
32. Sayed M, El-Maghraby H, Bondioli F, Naga S (2018) 3D carboxymethyl cellulose/hydroxyapatite (CMC/HA) scaffold composites based on recycled eggshell. J App Pharm Sci 8:023–030. http://dx.doi.org/10.7324/JAPS.2018.8304
33. Segal L, Creely JJ, Martin A Jr, Conrad C (1959) An empirical method for estimating the degree of crystallinity of native cellulose using the X-ray diffractometer. Text Res J 29:786–794. https://doi.org/10.1177%2F004051755902901003
34. Smičiklas I, Onjia A, Raičević S (2005) Experimental design approach in the synthesis of hydroxyapatite by neutralization method. Sep Purif Technol 44:97–102. https://doi.org/10.1016/j.seppur.2004.12.010
35. Tarus B, Fadel N, Al-Oufy A, El-Messiry M (2016) Effect of polymer concentration on the morphology and mechanical characteristics of electrospun cellulose acetate and poly (vinyl chloride) nanofiber mats. Alex Eng J 55:2975–2984. https://doi.org/10.1016/j.aej.2016.04.025

36. Turnbull G, Clarke J, Picard F et al (2018) 3D bioactive composite scaffolds for bone tissue engineering. Bioact Mater 3:278–314. https://doi.org/10.1016/j.bioactmat.2017.10.001
37. Zarei M, Samimi A, Khorram M et al (2021) Fabrication and characterization of conductive polypyrrole/chitosan/collagen electrospun nanofiber scaffold for tissue engineering application. Int J Biol Macromol 168:175–186. https://doi.org/10.1016/j.ijbiomac.2020.12.031
38. Zeng J, Haoqing H, Schaper A et al (2003) Poly-L-lactide nanofibers by electrospinning–Influence of solution viscosity and electrical conductivity on fiber diameter and fiber morphology. https://doi.org/10.1515/epoly.2003.3.1.102. e-Polymers 3
39. Zhang YP, Lynd LR (2004) Toward an aggregated understanding of enzymatic hydrolysis of cellulose: noncomplexed cellulase systems. Biotechnol Bioeng 88:797–824. https://doi.org/10.1002/bit.20282

Tables

Table 1

Taguchi's L_9 orthogonal array design along with electrospinning variables and their levels.

	Concentration (wt.%)	**Voltage (kV)**	**Flow rate (mL/h)**	**WD (cm)**
Level 1	1	20	0.5	10
Level 2	1.4	25	1	12
Level 3	1.6	30	1.5	15
Run no.	**Design**			
1	1	1	1	1
2	1	2	2	2
3	1	3	3	3
4	2	1	2	3
5	2	2	3	1
6	2	3	1	2
7	3	1	3	2
8	3	2	1	3
9	3	3	2	1

Table 2

Expected Taguchi's S/N ratio under optimum conditions.

Variable	Concentration	Voltage	Flow rate	WD
Effect size (Level)	16.1 (3)	5.3 (3)	1.1 (1)	1.9 (1)

Figures

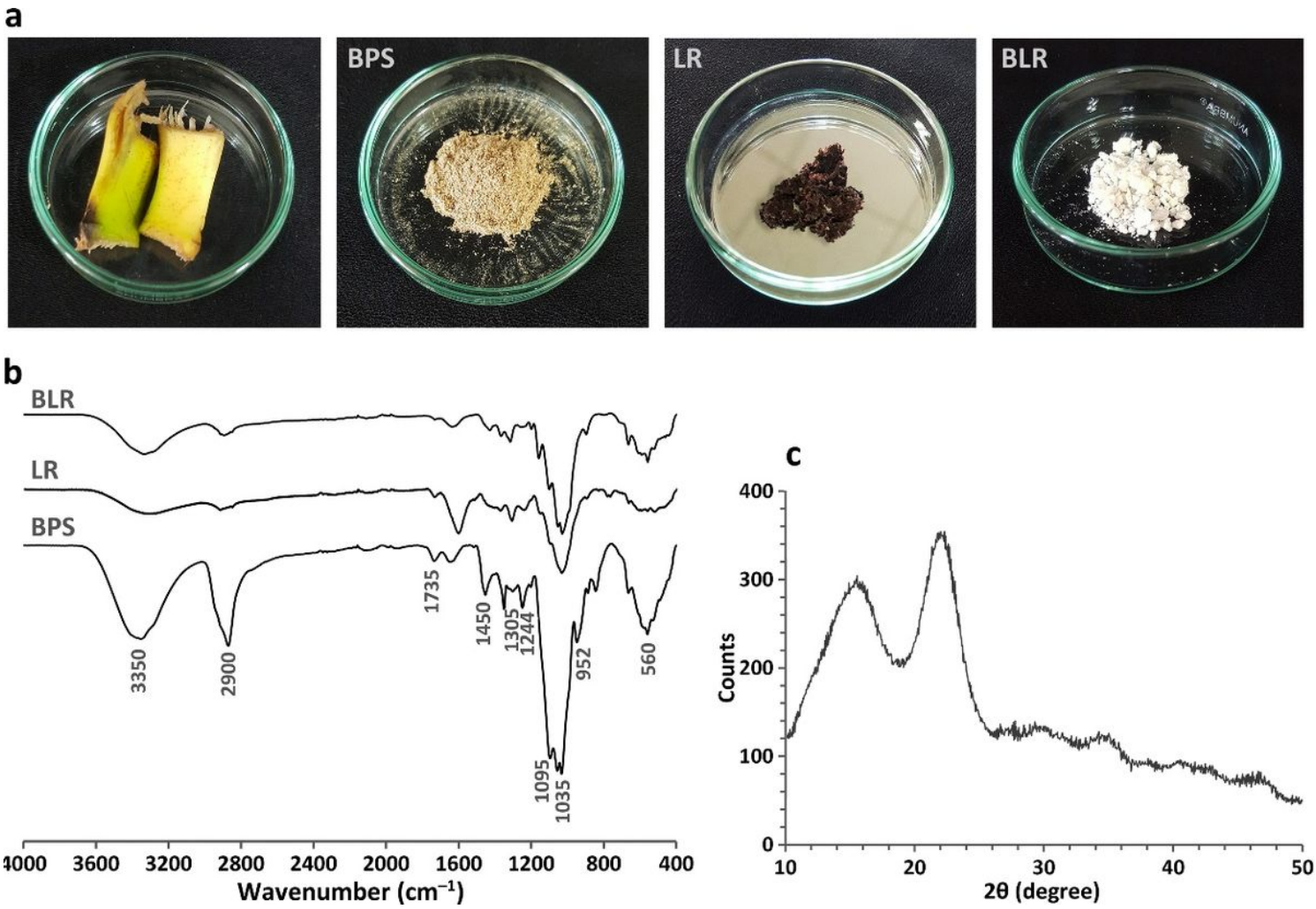

Figure 1

Structural characterizations of the as-extracted cellulose: (a) macroscopic appearance of BPS before milling (the first photo on the left), BPS powder, LR and BLR; (b) FTIR spectra recorded for BPS, LR and BLR; and (c) XRD pattern of BLR.

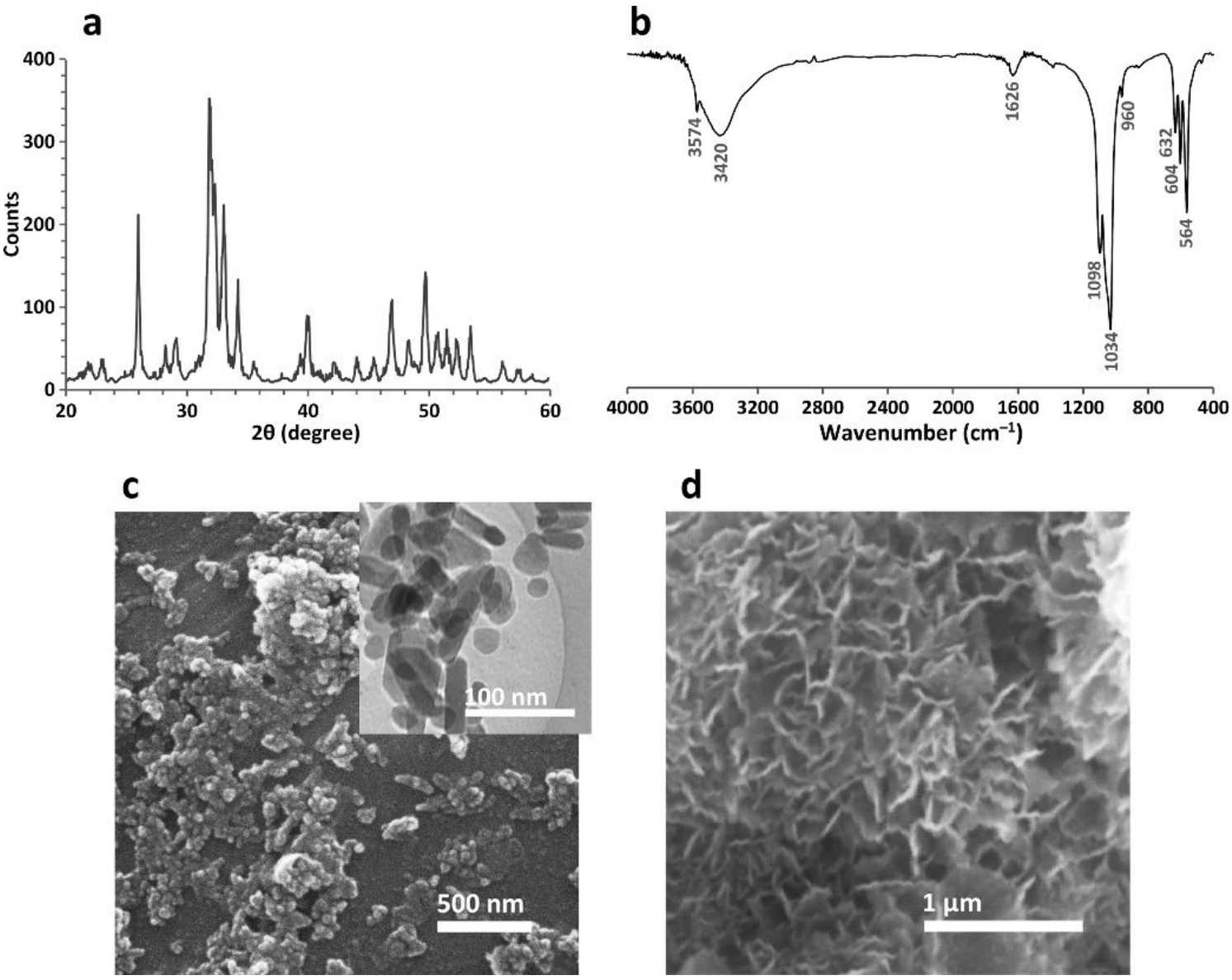

Figure 2

Characterizations of the as-synthesized HA nanoparticles: (a) XRD pattern; (b) FTIR spectrum; (c) SEM micrograph along with TEM micrograph (insert); and (d) SEM micrograph after a 30-day incubation of nanoparticles in SBF.

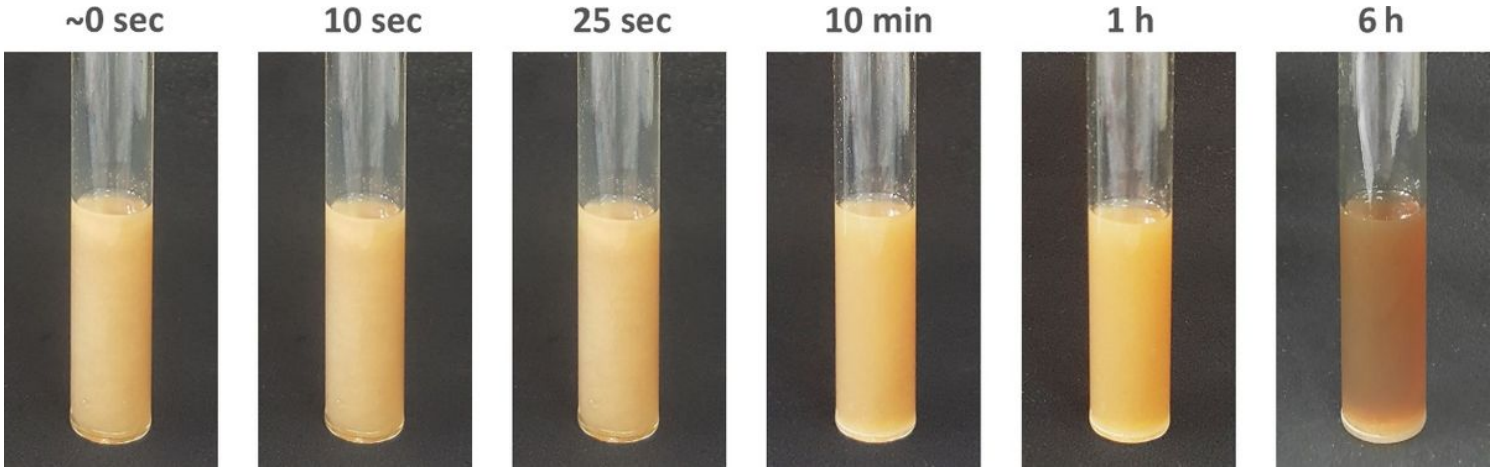

Figure 3

Monitoring of chemical and colloidal stability of HA nanoparticles dispersed in BLR/TFA solution during different time periods.

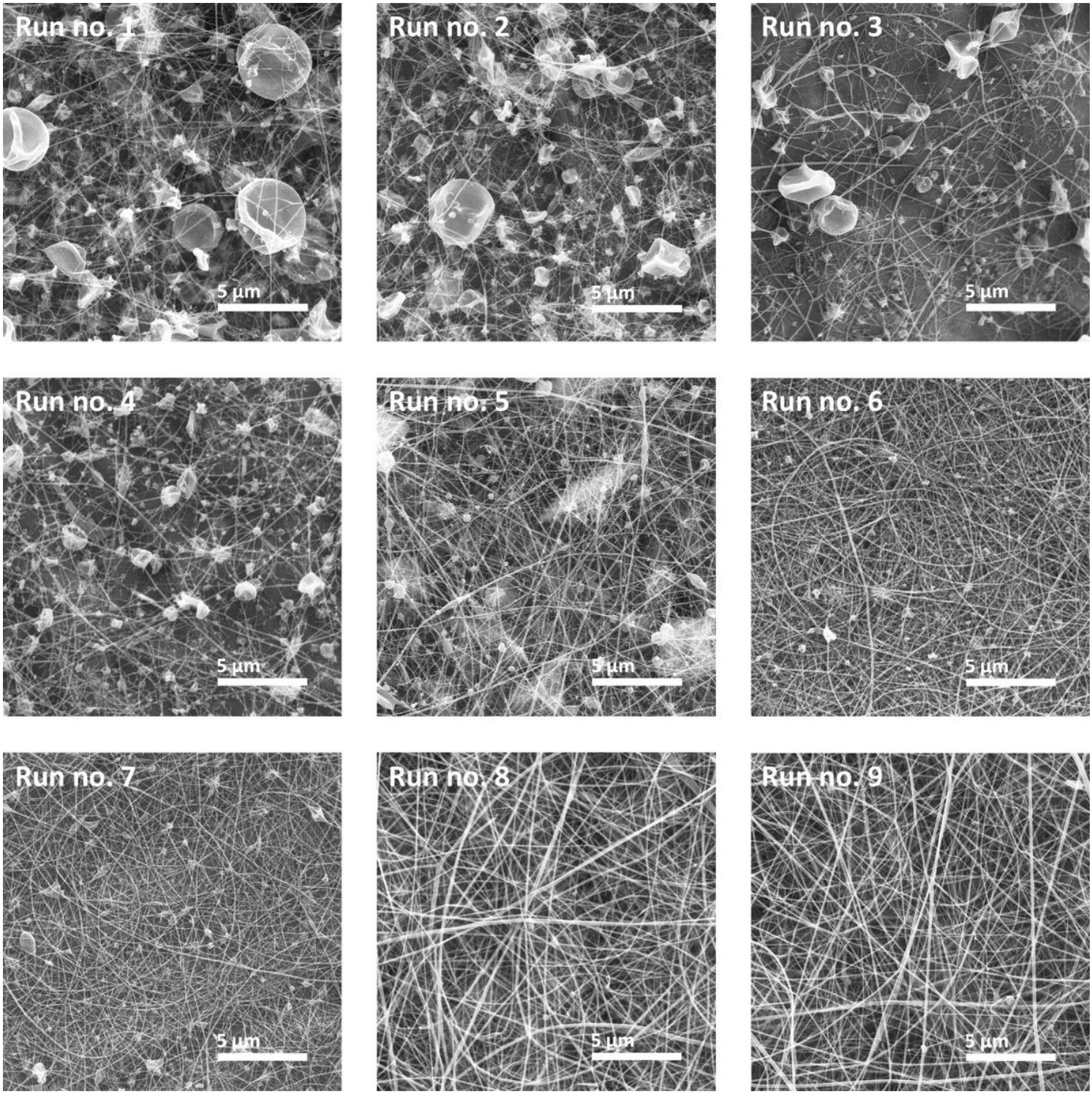

Figure 4

Representative SEM micrographs of fabricated cellulose nanofibers based on the Taguchi L9 orthogonal design.

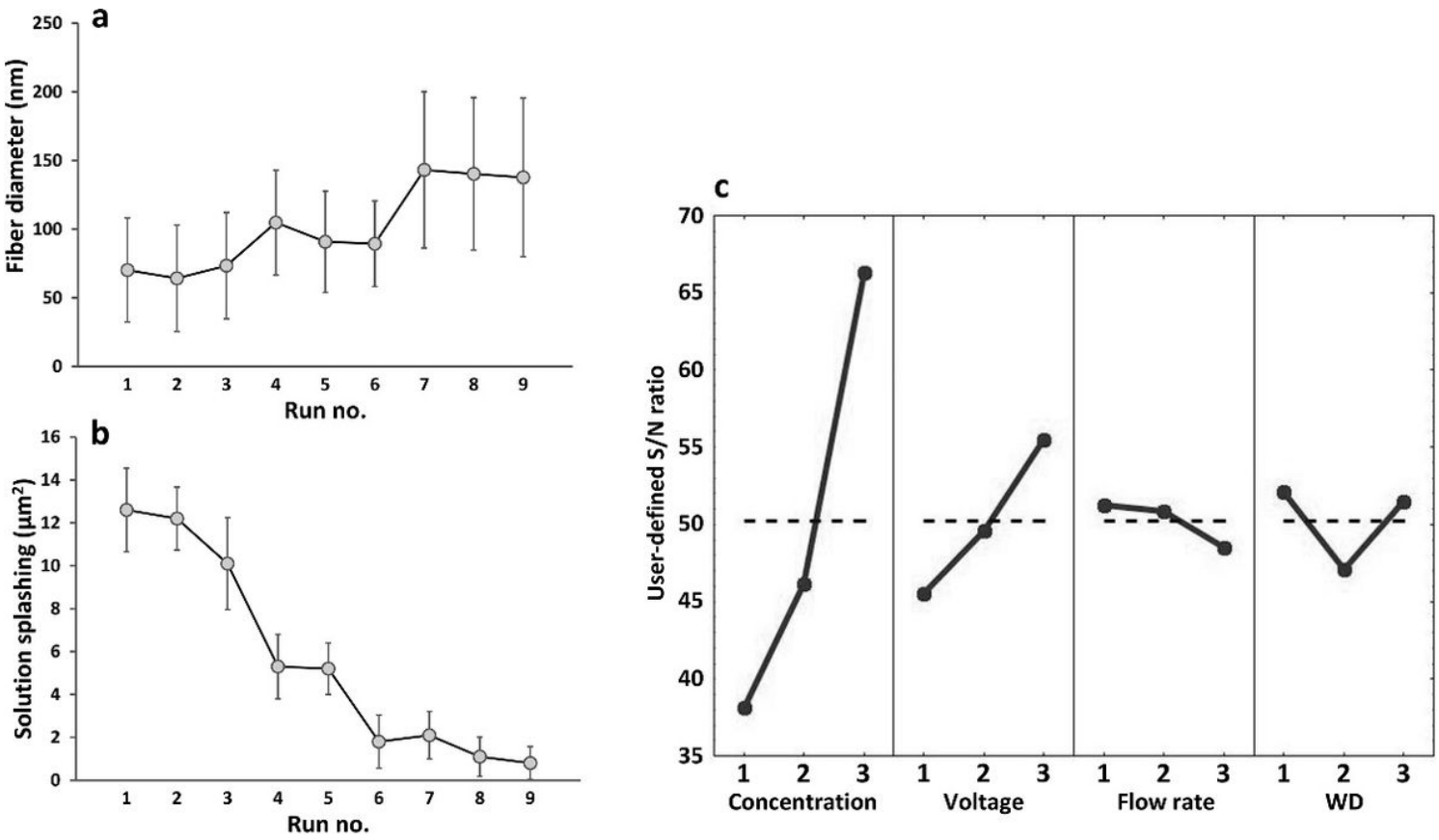

Figure 5

Diagram of average fiber diameter (a) and degree of splashing (b) by run no. (c) Mean plots of the level effect of each electrospinning variable.

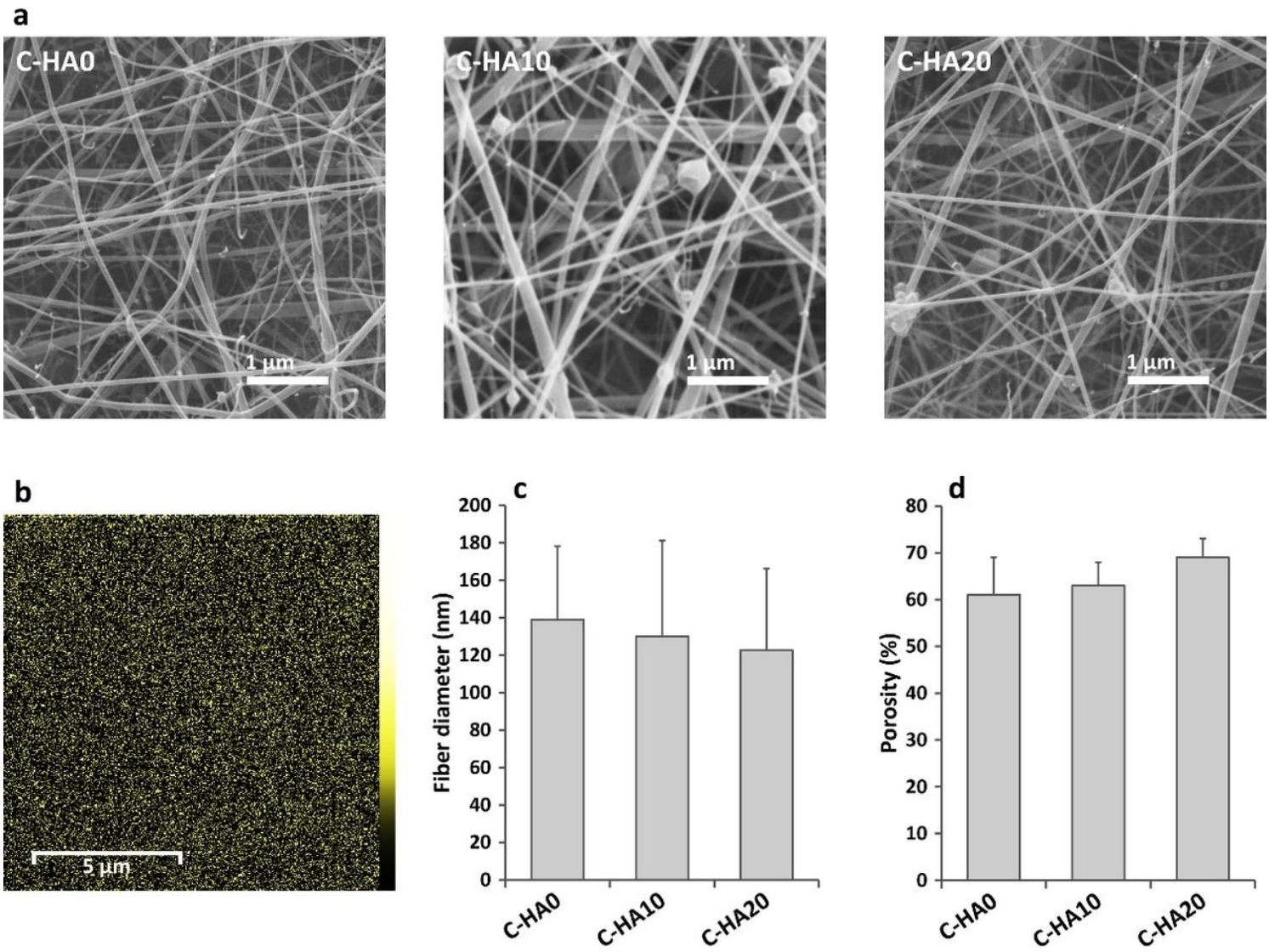

Figure 6

Morphological characterizations of fibrous cellulose/HA nanocomposites: (a) representative SEM micrographs of C-HA0, C-HA10, and C-HA20; (b) EDX-mapping of calcium ions present in the HA structure for C-HA20 nanocomposite; average fiber diameter (c) and average porosity of nanocomposites (d) containing different concentrations of HA nanoparticles.

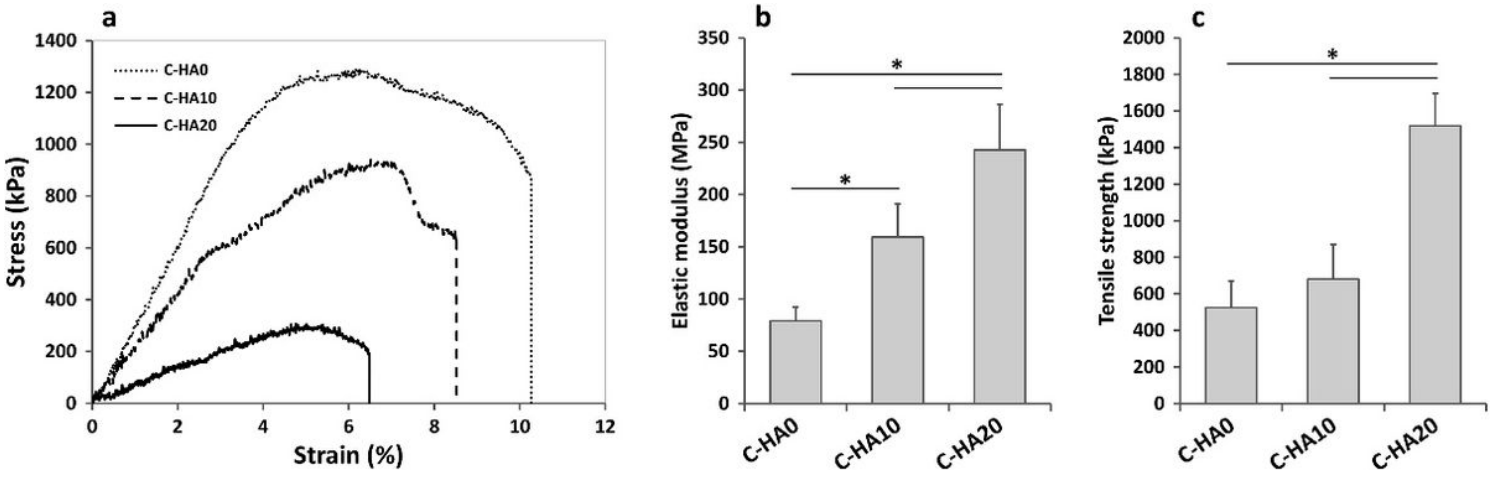

Figure 7

Mechanical characterizations of fibrous cellulose/HA nanocomposites: (a) representative stress–strain curves obtained for C-HA0, C-HA10, and C-HA20; elastic modulus (b) and tensile strength (c) of the cellulose/HA nanocomposites and control determined from the stress–strain curves; all results are mean ± SD of four measurements and the inserted asterisk (*) indicates a significant difference ($p < 0.05$) between the experimental groups.

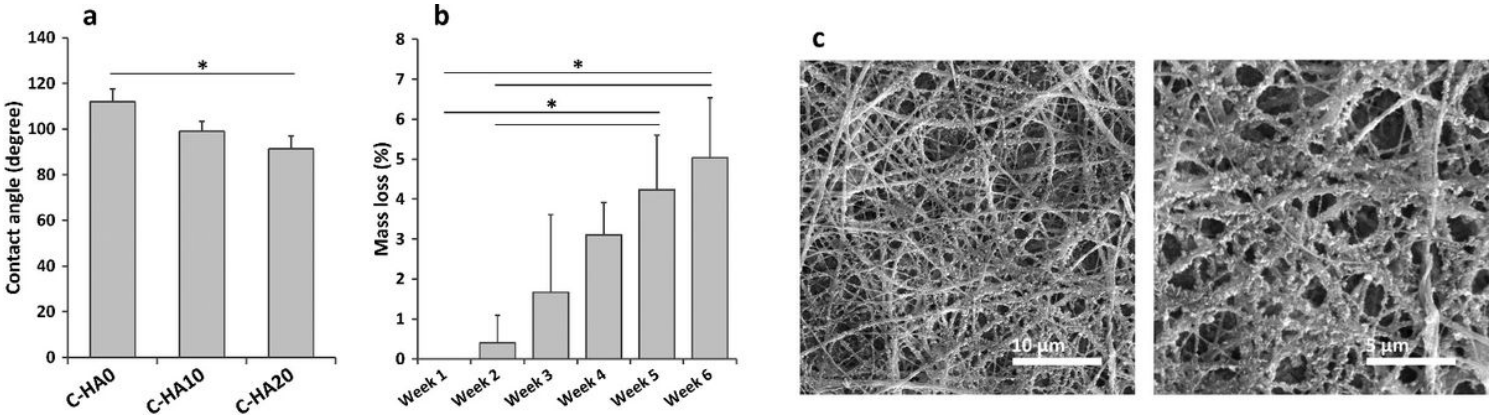

Figure 8

Biological characterizations of fibrous cellulose/HA nanocomposites: (a) estimation of average contact angle for C-HA0, C-HA10 and C-HA20; (b) biodegradability analysis of C-HA20 as function of degradation time; all results are mean ± SD of three measurements and the inserted asterisk (*) indicates a significant difference ($p < 0.05$) between the experimental groups; (c) SEM micrographs of C-HA20 nanocomposite at two different magnifications after 30 days of incubation in SBF at 37 °C.

Supplementary Files

This is a list of supplementary files associated with this preprint. Click to download.

- floatimage9.jpeg